Geophysica (2005), 41(1-2), 31-55

MERIS, MODIS and ETM+ Channel Configurations in the Estimation of Lake Water Quality from Subsurface Reflectance Using Semi-analytical and Empirical Algorithms

Kari Kallio[1], Jouni Pulliainen[2] and Pasi Ylöstalo[3]

[1]Finnish Environment Institute, P.O. Box 140, FIN-00251 Helsinki, Finland

[2]Laboratory of Space Technology, P.O. Box 3000, FIN-02015 Espoo, Finland

[3]Finnish Institute of Marine Research, P.O. Box 2, FIN-00561 Helsinki, Finland

(Received: September 2004; Accepted: July 2005)

Abstract

We studied the estimation of lake water quality from measured subsurface reflectances in order to find out the potential of the channel configurations of three satellite instruments (MERIS, MODIS and ETM+). The semi-analytical method was based on the inversion of a bio-optical reflectance model and the empirical method on using channel ratios or single channels. The dataset, consisting of data from 11 lakes located in Finland, has a wide range of water quality: the sum of chlorophyll a *and phaeophytin* a *($C_{Chl\text{-}a}$) ranging from 0.8 to72 $\mu g\ l^{-1}$, total suspended solids (C_{TSS}) from 0.4 to 24 mg l^{-1} and the absorption coefficient of CDOM at 400 nm ($a_{cdom}(400)$) from 0.4 to 14 m^{-1}. The results from the inversion method indicate that MODIS and MERIS have nearly optimum channel configurations for the estimation of C_{TSS} and $a_{cdom}(400)$ in the lakes we studied. The analyses of the empirical algorithms suggest that MERIS has optimum channels for water quality estimations. The estimation accuracy of C_{TSS} and $C_{Chl\text{-}a}$ by the MERIS and MODIS configurations was about the same for the two estimation methods, but in case of $a_{cdom}(400)$ the empirical algorithms were clearly better than the inversion method. $a_{cdom}(400)$ was estimated using ETM+ channels with about the same accuracy as by MERIS and MODIS channels.*

Key words: reflectance, water quality, inversion, channel ratios, lakes, remote sensing

1. Introduction

Interpretation of water quality from remote sensing data is often based on empirical algorithms where water quality variables are estimated from the reflectance at one wavelength or from ratios between reflectances measured at two wavelengths. Empirical estimation methods can be divided into purely empirical and semi-empirical algorithms. Semi-empirical algorithms rest on the knowledge on how the optical properties of optically active variables affect the reflectance at the applied wavelengths. Chlorophyll *a*, for example, can be estimated with the blue/green reflectance ratio in the case

of oceans (*O'Reilly et al.,* 1998) and with NIR/red ratio (*Gitelson et al.,* 2002; NIR=near-infrared) in lakes. Both algorithms utilize the absorption maximums of phytoplankton located at about 440 and 675 nm.

Empirical methods have particularly proved applicable to clear ocean waters, but in lakes and coastal waters the estimation of one water quality variable is often disturbed by other optically active substances (OAS). One way to solve this problem in these 'case 2' waters is to use interpretation methods that are based on bio-optical modeling. Such models calculate the reflectance from the specific inherent optical properties (SIOPs) and from the concentrations of optically active substances. Estimation of water quality using bio-optical reflectance modelling is usually based on the inversion of the applied model. The inversion method has been used in coastal and ocean applications (see e.g. *Doerffer & Fischer,* 1993*; Garver & Siegel,* 1997; *Schiller and Doerffer,* 1999; *Maritorena et al.,* 2000; *Lee and Carder,* 2004) as well as in lake applications (e.g. *Bukata et al.,* 1981*, Gege,* 1998; *Kutser et al.,* 2001; *Pierson and Strömbeck,* 2001). The problem of increased computing time due to pixel-by-pixel inversion of hyperspectral satellite images has been solved by the use of neural networks (e.g. *Schiller and Doerffer,* 1999) and by matrix inversion (*Hoge and Lyon,* 1996; *Hoogenboom et al.,* 1998b). *Gons* (1999) used a combination of bio-optical modeling and a channel ratio in the estimation of chlorophyll-a in eutrophic lakes. The advantages of using bio-optical modeling in the interpretation are 1) all channels of the remote sensing instrument are utilized and 2) regional, seasonal and water type differences in the SIOPs can be considered in the interpretation.

The aim of this paper was to investigate the suitability of the channel configurations of three satellite instruments for the estimation of OAS concentrations of lakes using the inversion method and empirical algorithms. The studied OAS consisted of chlorophyll *a*, total suspended solids and coloured dissolved organic matter (CDOM). The analyses were based on the measured subsurface reflectance spectra from which reflectances were constructed for each satellite instrument channel. The channel configurations included in the study consisted of two ocean color instruments (ENVISAT MERIS, TERRA/AQUA MODIS) together with LANDSAT ETM+. MODIS and MERIS are multispectral instruments having similar channel configuration in the VIS(visible)-NIR range of the spectrum with the exception that MERIS has channels at 620 and 705 nm, which are not found in MODIS. ETM+ has three wide channels in VIS. Although ETM+ was designed for land applications it has also been used in water quality studies of lakes (e.g. *Kloiber et al.,* 2002, *Vincenta et al.,* 2004) and coastal waters (e.g. *Lavery et al.,* 1993) due to its good spatial resolution (30 m). Many of the published water quality algorithm studies of lakes have focused on one estimation method or on one lake type only. For our study we selected 11 lakes, displaying a range of varying lake type (oligotrophic – eutrophic, humic). The semi-analytical bio-optical reflectance model needed in inversion was first parametrized using SIOP's measured in the field and laboratory.

2. *Material and methods*

2.1 *Description of lakes*

Optical and limnological measurements were carried out in 1997 and 1998 at 14 stations representing 11 lakes located in southern and northern Finland (Table 1). Five of the stations were surveyed both in May and in July-August. Each lake had one measurement station with the exception of Lake Norvajärvi and Lake Pääjärvi, each of which had two stations, and of Lake Lohjanjärvi, where there were three stations in May and four stations in August. The reflectance spectra of 12 stations were used in model testing and in the estimation of OAS. The remaining reflectance spectra were not accepted for further analyses due to noise caused by waves or large variations in incoming solar radiation. However, the SIOPs of all stations were utilized in the parametrization of the reflectance model. The OAS concentrations and optical properties of the stations are presented in Table 2.

Table 1. Main characteristics of the lakes studied. Number of stations and measurement months are also given. Each lake was sampled at one station with the exception of Lohjanjärvi (4 stations), Pääjärvi (2 stations) and Norvajärvi (2 stations). Oligo = oligotrophic, Meso = mesotrophic, Eu = eutrophic, S. Finland = southern Finland, N. Finland = northern Finland.

Lake	Short name	Region	Coordinates	Area km^2	z_{max} m	Lake type	Month
Enäjärvi, Vihti	Ena	S. Finland	60°20'N 24°23'E	5	3.4	Eu	Aug.
Lohjanjärvi	Loh	S. Finland	60°15'N 23°55'N	94	12.6	Meso-Eu	May, Aug.
Vesijärvi, Lahti	Ves	S. Finland	61°02'N 25°37'E	111	41	Meso	Aug.
Puujärvi	Puu	S. Finland	60°15'N 23°45'E	7	21	Oligo	May, Aug.
Pääjärvi	Pää	S. Finland	61°5'N 25°10'E	13.1	85	Humic	Aug.
Keravanjärvi	Ker	S. Finland	60°37'N 25°5'E	1	2.2	Humic	May
Vasikkajärvi	Vas	N. Finland	67° 7'N 26° 5'E	0.3	17	Oligo	July
Norvajärvi	Nor	N. Finland	66°37'N 25°47'E	11	15	Oligo	July
Pöyliöjärvi	Pöy	N. Finland	66°27'N 25°48'E	1.3	8	Humic	July
Sonkajärvi	Son	N. Finland	66°37'N 25°14'E	3.2	11	Humic	July
Sierijärvi	Sie	N. Finland	66°28'N 25°57'E	4	2.5	Eu	July

The lakes were classified (Table 1) according to *OECD* (1982) based on the maximum chlorophyll *a* concentration (values measured in July-August in this study):

- oligotrophic ($C_{Chl\text{-}a}(max) \leq 8\ \mu g\ l^{-1}$)
- mesotrophic ($8\ \mu g\ l^{-1} < C_{Chl\text{-}a}(max) \leq 25\ \mu g\ l^{-1}$)
- eutrophic ($C_{Chl\text{-}a}(max) > 25\ \mu g\ l^{-1}$)

Humic lakes, characterized by the high concentration of CDOM and the relatively low concentration of total suspended solids and chlorophyll *a*, were separated from the rest of the lakes ($a_{cdom}(400)>4.0\ m^{-1}$ and $C_{Chl\text{-}a}(max)< 8\ \mu g\ l^{-1}$).

Table 2. The concentrations of OAS, Secchi depth, K_d(PAR), a_{tot}(412) and b_{tot}(555) of the stations. a_{tot}(412) and b_{tot}(555) were measured with ac-9 and are presented without pure water.

Station	Month	C_{TSS} mg l^{-1}	C_{Chl-a} µg l^{-1}	a_{cdom}(400) m^{-1}	Secchi m	K_d(PAR) m^{-1}	a_{tot}(412) m^{-1}	b_{tot}(555) m^{-1}
Puu-m*	May	1.9	4.5	2.1	3.9	1.1	2.0	1.2
Loh1-a*	Aug.	15.5	55	5.3	0.8	3.8	6.2	6.6
Loh2-a*	Aug.	4.6	13.5	3.8	1.5	1.9	3.6	2.6
Loh3-a*	Aug.	5.9	10.5	3.9	1.9	2.0	3.5	2.5
Loh4-a*	Aug.	3.0	11.5	3.3	2.9	1.	3.1	1.9
Ena-a*	Aug.	10	37	1.9	1.1	2.8	3.7	7.9
Nor1-a*	Aug.	0.8	3.5	3.1	4.0	1.5	2.9	1.0
Nor2-a*	Aug.	1.1	3.3	3.6	3.3	1.5	2.9	0.9
Sie-a*	Aug.	19.6	73	18.2	0.4	7.8	-	-
Sin-a*	Aug.	1.7	5.7	13.0	2.2	3.9	10.6	1.7
Poy-a*	Aug.	1.0	7.6	10.0	2.5	3.0	8.4	1.2
Vas-a*	Aug.	0.4	0.8	0.3	11.8	0.6	0.4	0.3
Loh1-m	May	17	9.7	9.2	0.8	-	7.5	8.1
Loh2-m	May	10	7.2	5.4	1.1	-	5.2	4.5
Loh3-m	May	7.8	4.2	4.8	1.2	-	4.5	3.6
Ker-m	May	4.4	8.8	14.3	1.4	-	12.5	2.8
Puu-a	Aug.	1.7	1.3	1.3	7.0	0.8	1.2	0.9
Ves-a	Aug.	2	11.5	1.4	2.8	-	1.7	2.1
Paa1-a	Aug.	2.1	5.5	7.4	2.7	-	6.1	1.4
Paa2-a	Aug.	1.6	6.8	7.2	2.7	2.7	6.2	1.4

* Stations used for testing the bio-optical reflectance model and the water quality algorithms. All stations were utilized in model parametrization.

2.2 Limnological and optical measurements

Water samples were taken from depths of 0–0.4 and 0.8–1.2 m. In the subsequent analyses the average concentrations of these two depths were used. Water quality determinations of the samples were made in the water laboratories of the Regional Environment Centres of Uusimaa and of Lapland. Concentration of total suspended solids (C_{TSS}) was measured using gravimetric determination of the matter removed by a filter (*EN 872*, Nuclepore polycarbonate 0.4 µm filter). Concentration of the sum of chlorophyll *a* and phaeophytin *a* (C_{Chl-a}) was determined with a spectrophotometer after their extraction using hot ethanol (*ISO 10260*, GF/C filter). The absorption spectra (380–800 nm) of CDOM were measured with a spectrophotometer (5 cm long cuvette) from a sample filtered through a Nuclepore polycarbonate 0.4 µm filter. The absoption measurements were corrected for residual scattering (due to small particles not retained by the filter) by subtracting absorption at 750 nm from the measured values in 400-750 nm (*Gallie,* 1994). The absorption coefficient at 400 nm (a_{cdom}(400)) was used as a measure of CDOM concentration. Phytoplankton species and phytoplankton biomass were determined by microscopic counting.

The optical measurements conducted from a boat consisted of upwelling and downwelling irradiances (Li1800UW underwater spectrometer, LI-COR Corporation), and total absorption and attenuation coefficients (ac-9 absorption/attenuation meter, WET Labs Inc.). Downwelling and upwelling spectral irradiance (300–850 nm with a step of 2 nm) were measured at depths of 0.5, 1, 2 and 3 m. The Li18000UW was kept away (about 1.5 m) from the boat by a boom. To measure the upwelling irradiance, the Li1800UW instrument was turned around with the detector facing downward. The long integration period (40 s) resulted in noisy irradiance spectra, particularly in windy conditions. To remove this intensity variation due to wave focusing, the spectra were smoothed by the Butterworth recursive filter method. Variation in the global radiation (i.e. direct solar plus diffuse sky radiation) between upwelling and downwelling irradiance measurements may result in erroneous reflectance. Because of this, the underwater irradiances were corrected by the ratio between the average incident irradiance above the water surface during one measurement series (duration about 30 minutes) and the incident irradiance corresponding to the time of each underwater spectrum measurement (*Herlevi,* 2002). The incident irradiance (400–1100 nm) above the water surface was recorded with a Li200SA sensor.

The underwater reflectances (R) were calculated by dividing the upwelling irradiance (E_u) by the downwelling irradiance (E_d) at each depth:

$$R(z_i,\lambda)=\frac{E_u\ (z_i,\lambda)}{E_d\ (z_i,\lambda)} \tag{1}$$

In the subsequent analyses we mainly used reflectances measured at the depth of 0.5 m.

The diffuse attenuation coefficient K_d was calculated from downwelling irradiances E_d measured by the Li1800UW underwater spectrometer at the depths of 0.5 and 1.0 m:

$$K_d(z,\lambda)=\frac{1}{z_2-z_1}\ln\left[\frac{E_d\ (z_2,\lambda)}{E_d\ (z_1,\lambda)}\right] \tag{2}$$

where z is water depth. $K_d(PAR)$ was obtained by calculating the mean K_d of the 400-700 nm region and it ranged between 0.6 and 7.8 m^{-1} (Table 2).

The wavelengths used in the ac-9 absorption/attenuation meter were 412, 440, 488, 510, 532, 555, 650, 676 and 715 nm. The measurements were performed as depth profiles of the whole water column by lowering the instrument at a steady speed from the boat. Typically, three profiles were measured at each station. In the further analyses of the data, we used the average values of the measurements taken from 0–2 m. The obtained values were corrected for temperature and scattering according to the ac-9 manual (*WET Labs*, 1995). The total scattering coefficient was obtained as the difference between the corrected attenuation and absorption coefficient.

2.3 Structure of the bio-optical model

Calculation of irradiance reflectance just beneath the water surface, R(0-,λ), is based on the following equation (*Gordon et al.,* 1975 and simplified by *Jerlov,* 1976):

$$R\ (0-,\lambda) = C\frac{b_{b,Tot}(\lambda)}{a_{Tot}(\lambda)+b_{b,Tot}(\lambda)} \tag{3}$$

where $b_{b,\,Tot}(\lambda)$ is the total backscattering coefficient and $a_{Tot}(\lambda)$ is the total absorption coefficient. *C* depends mainly on the illumination and viewing geometry. Here C was estimated by the equation presented by *Kirk* (1984):

$$C = -0.629\mu_0 + 0.975 \tag{4}$$

where μ_0 is the cosine of the solar zenith angle in the water. The model simulates reflectance in the 400-750 nm range with a step of 2 nm. Utilizing Beer's law $a_{Tot}(\lambda)$ and $b_{b,\,Tot}(\lambda)$ in Eq. (3) are obtained by summing up the absorption and backscattering coefficients of the optically active substances in the water.

Similar bio-optical reflectance models to the one described here have been widely used in lake water quality studies (e.g. *Bukata et al.,* 1981; *Dekker,* 1993; *Hoogenboom et al.,* 1998a; *Kondratyev et al.,* 1998; *Podznyakov et al.,* 1998; *Pierson and Strömbeck,* 2000). The main differences between the models are the number of the optically active substances included and the numerical values of the specific inherent optical properties. We assumed four optically active components in the model: phytoplankton, tripton, colored dissolved organic matter and pure water. Tripton is non-living particulate matter and it mainly consists of detritus and inorganic particles. Total backscattering was calculated without considering phytoplankton and tripton backscattering separately.

The total spectral absorption coefficient is described by:

$$a_{Tot}(\lambda) = a_w(\lambda) + a_{cdom}(\lambda) + a_{Ph}(\lambda) + a_{Tri}(\lambda) \tag{5}$$

where $a_w(\lambda)$ is the absorption coefficient of pure water (*Buiteveld,* 1994), $a_{Ph}(\lambda)$ is the absorption coefficient of phytoplankton, $a_{cdom}(\lambda)$ is the absorption coefficient of CDOM and $a_{Tri}(\lambda)$ is the specific absorption coefficient of tripton.

Absorption by CDOM is calculated by assuming an exponential increase with a decreasing wavelength (*Bricaud et al.,* 1981):

$$a_{cdom}(\lambda) = a_{cdom}(400)\, e^{-S_{cdom}(\lambda-400)} \tag{6}$$

where $a_{cdom}(400)$ is the absorption coefficient of CDOM at 400 nm and S_{CDOM} is the slope factor.

Absorption by phytoplankton, $a_{Ph}(\lambda)$, is calculated by:

$$a_{Ph}(\lambda) = a^*_{Ph}(\lambda) C_{Chl-a} \tag{7}$$

where $a^*_{Ph}(\lambda)$ is the Chl-a specific absorption coefficient of phytoplankton.

Absorption by tripton, $a_{Tri}(\lambda)$, is expressed as:

$$a_{Tri}(\lambda) = a^*_{\underline{TSS}}(\lambda) C_{TSS} \tag{8}$$

where is $a^*_{\underline{TSS}}(\lambda)$ the specific absorption of bleached total suspended solids and C_{TSS} is the concentration of TSS. Here we define absorption by tripton using C_{TSS}, because tripton concentration measurements were not available. $a^*_{TSS}(\lambda)$ is described analogous to the calculation of $a_{cdom}(\lambda)$ (*Roesler et al.,* 1989):

$$a^*_{\underline{TSS}}(\lambda) = a^*_{\underline{TSS}}(400)\, e^{-S_{Tri}(\lambda - 400)} \tag{9}$$

where $a^*_{\underline{TSS}}(400)$ is the specific absorption of bleached total suspended solids at 400 nm and S_{Tri} is the slope factor of tripton absorption.

The total backscattering coefficient $b_{b,Tot}(\lambda)$ is described by:

$$b_{b,tot}(\lambda) = bp_w b_w(\lambda) + bp_{TSS} b^*_{TSS}(\lambda) C_{TSS} \tag{10}$$

where b_w is the scattering coefficient of pure water (*Buiteveld,* 1994), and b^*_{TSS} is the specific scattering coefficient of TSS. The backscattering probability of pure water, bp_w, was set at 0.5 (*Sathyendranath et al.,* 1989). bp_{TSS} is the backscattering probability of TSS.

We assumed that the specific scattering coefficient of TSS ($b^*_{TSS}(\lambda)$) can be described by a power function:

$$b^*_{TSS}(\lambda) = b^*_{TSS}(555)\left(\frac{555}{\lambda}\right)^{n_b} \tag{11}$$

where $b^*_{TSS}(555)$ is the specific scattering coefficient of TSS at 555 nm and n_b is the scattering exponent.

2.4 Estimation of model coefficients

Our aim was to develop a reflectance model applicable for the lake types typical to Finland. The most important monitoring period during ice-free conditions in Finland is July–August. This because of the phytoplankton biomass, the occurrence of cyanobacteria and the low oxygen concentrations in the hypolimnion. Therefore, we mainly used the SIOPs from July-August in the model parametrization. The SIOPs in spring can be different from those in the period July-August due to distinct phytoplankton species and material discharge from the watershed during spring flooding.

The Chl-a specific absorption coefficient of phytoplankton, a^*_{Ph} in Eq. (7), was calculated using the power function originally presented by *Bricaud et al.* (1995):

$$a^*_{Ph}(\lambda) = A(\lambda) C_{Chl}^{-B(\lambda)} \tag{12}$$

where $A(\lambda)$ and $B(\lambda)$ are positive empirical coefficients. *Bricaud et al.* (1995) published the average coefficients based on ocean data. Here $A(\lambda)$ and $B(\lambda)$ were obtained from a study of *Ylöstalo et al.* (2005) carried out in 2000 and 2002 at 10 Finnish lakes. Three of the lakes and five of the station in our study were the same as in *Ylöstalo et al.* (2005). According to Eq. (12) a^*_{Ph} decreases from oligotrophic to eutrophic waters. This is due to the package effect and the possible systematic changes between species composition/pigmentation and trophic level (*Bricaud et al.,* 1995). The specific absorption coefficient of bleached total suspended solids ($a^*_{TSS}(400)$) and the slope factor of tripton absorption (S_{Tri}) were also taken from the study by *Ylöstalo et al.* (2005).

The slope factor S_{cdom} was estimated by fitting Eq. (6) to the measured $a_{cdom}(\lambda)$ (18 spectra, wavelength range used in the optimization was 400-750 nm). Two lakes were excluded from the optimization: Lake Sierijärvi (high scattering in the long wavelength region because of ineffective filtering) and Lake Vasikkajärvi (noisy absorption spectrum arising from a cuvette that was too short for this clear water lake). The S_{cdom} obtained through optimization was 0.0150 nm^{-1}. The variation of S_{cdom} in different lakes/stations was small (standard deviation = 0.000902 or 5.8% of the mean, min = 0.0136 nm^{-1}, max = 0.0175 nm^{-1}).

The specific scattering coefficient, $b^*_{TSS}(555)$, and the scattering exponent, n_b, were estimated from the ac-9 measurements. The specific scattering coefficient ($b^*_{TSS}(\lambda)$) was calculated for the nine ac-9 wavelengths by:

$$b^*_{TSS}(\lambda) = \frac{b_{Tot}(\lambda) - b_w(\lambda)}{C_{TSS}} \tag{13}$$

where $b_{Tot}(\lambda)$ is the total scattering measured with the ac-9. The mean value of the $b^*_{TSS}(555)$ was 0.811 l m^{-1} mg^{-1} (mean of August without Sie-a and Puu-a, n=13, the name abbreviations are explained in Table 1 and Table 2) and the scattering coefficient n_b obtained through optimization against the measured $b^*_{TSS}(\lambda)$ was 0.70 (August without Sie-a, n=14). Sie-a was excluded from the estimations because of the non-linearity in the ac-9 measurements. The reliable measurement of a and b with ac-9 in this very eutrophic lake would require a shorter optical pathlength than the 25 cm used in our study (ac-9 is available also with 10 cm pathlength, *WET Labs,* 1995). In waters with high c the 25 cm pathlength results in poor resolution and unreliable a and b.

In addition, the backscattering ratios are needed for the calculation of $b_{b,Tot}$ (Eq. 10). The backscattering probability of TSS (bp_{TSS}) was estimated by fitting the modeled reflectance spectrum (Eq. 3) with the 12 reflectance spectrum measured with the LI-1800UW. The 400–448 nm range was not included in the analyses, because of the difficulties in measuring the low irradiance levels and possible instrument self-shading in the blue end of the spectrum. We assumed the backscattering ratios to be constant over the whole wavelength range. All the optimized coefficients (S_{CDOM}, n_b, bp_{TSS}) were determined with least-squared method using the Nelder-Mead simplex search technique (*Nelder and Mead,* 1965).

2.5 Estimation of water quality

The applicability of the channel configurations of MERIS, MODIS (1 km data) and ETM+ for the estimation of OAS were tested using the inversion technique and the empirical algorithms. For these experiments reflectances were averaged for the satellite instrument channels (Table 3). The wavelength range used in the inversion and empirical methods was 450-750 nm. For this reason the MODIS channel 8 (743–753 nm) and the MERIS channel 10 (750–757.5 nm) were replaced by 744–750 nm. Channel 2 (438–448 nm) of MERIS and MODIS was replaced by 450–460 nm. In addition, we examined whether the use of the full reflectance spectrum (450–750 nm with a step of 2 nm) improved the estimation accuracy of OAS. Before the empirical analyses using the full spectrum the 10 nm moving averages were calculated for every R(λ).

Table 3. Channels of ETM+, MODIS (1 km data) and MERIS satellite instruments in the 400-760 nm range. The same channels (except MODIS and MERIS channel 1) were used in the OAS estimations.

Channel number	Wavelength range nm		
	ETM+	MODIS	MERIS
1	450-520	405-420	407.5-417.5
2	530-610	438-448 (this study: 450-460)	437.5-447.5 (this study: 450-460)
3	630-690	483-493	485-495
4		526-536	505-515
5		546-556	555-565
6		662-672	615-625
7		673-683	660-670
8		743-753 (this study: 743-750)	677.5-685
9			700-710
10			750-757.5 (this study: 743-750)

The applied inversion method is based on the maximum likelihood method assuming that the forward (reflectance) modeling error is normally distributed. Following this, the maximum likelihood estimate for multiple variables is obtained by searching the maximum value of a multi-dimensional Gaussian conditional probability density distribution. When the modeling errors of different channels are assumed to be independent from each other, the obtained constrained minimization problem for the joint estimation of C_{TSS}, $C_{Chl\text{-}a}$ and $a_{cdom}(400)$ is:

$$\min_{\text{TSS, Chl−a, a400}} \sum_{i=1}^{n} \frac{1}{2\sigma_i^2} \left(R_{\text{i,sim}} - R_{\text{i,mea}}\right)^2 \tag{14}$$

$$\text{with respect to constraints}: 0.2 \le C_{TSS} \le 25 \text{ mg l}^{-1}, 0.2 \le C_{Chl\text{-}a} \le 100 \text{ µg l}^{-1} \text{ and}$$

$$0.2 \le a_{cdom}(400) \le 25 \text{ m}^{-1}$$

where σ_i is the standard deviation of statistical reflectance modeling error for channel *i*. $R_{i,sim}$ and $R_{i,mea}$ are the simulated and measured reflectances for channel i, respectively. σ_i is estimated using the root mean squared error (rmse), which is calculated from the residual errors between the measured and simulated reflectances (Eq. 16). The simulated reflectances for the 12 stations were obtained using measured C_{TSS}, $C_{Chl\text{-}a}$ and $a_{cdom}(400)$ as model input. In practice, each inverse variance term, σ_i^{-2}, weights each channel according to its estimated modeling accuracy. Eq. (14) can be used with any spectral channel configuration or using averaged channels. However, the minimum number of channels (*n*) has to be as high as the number of estimated variables in order to avoid an ill-posed inversion problem.

The best empirical algorithms were identified by calculating correlations of C_{TSS}, $C_{Chl\text{-}a}$ and $a_{cdom}(400)$ with all R(λ) (450–750 nm with a step of 2 nm) and all possible ratios of two R(λ). The general formulation of the empirical algorithms was:

$$C_i = a\,X + b \tag{15}$$

where C_i is the concentration of variable i, *a* and *b* are empirical parameters and *X* is an independent variable (reflectance of a single channel or reflectance ratio of two channels).

The accuracy characteristics of the model and OAS algorithms were defined by R^2 and root mean squared error (rmse), which is defined as:

$$rmse = \sqrt{\frac{1}{N-p}\sum_{i=1}^{N}(\hat{Y}_i - Y_i)^2} \tag{16}$$

where $\hat{Y}_i$ is the estimated value and Y_i is the measured value. p=0 in calculating the residual error of the optimization problem (Eq. 14) and in calculating rmse of the inversion estimates, and p=2 for the empirical algorithms. The relative rmse (%) was calculated from the rmse and the measured average value.

3. Results

3.1 Bio-optical reflectance model

The simulated (Eq. 5) and measured (ac-9) a_{tot} are presented in Fig. 1. At three Lohjanjärvi stations (Loh1-a, Loh2-a, Loh3-a), the simulated a_{tot} is slightly higher than the measured a_{tot}. The specific backscattering coefficient at 555 nm ($b^*_{b,TSS}(555) = bp_{TSS} \cdot b^*_{TSS}(555)$) was estimated by optimizing the backscattering probability (bp_{TSS}) of the reflectance model. This resulted in bp_{TSS}=0.0131, corresponding to $b^*_{b,TSS}$ (555) of 0.0106 l m^{-1} mg^{-1}. The model coefficient are summarized in Table 4. The simulated and measured reflectances for the 12 stations are shown in Fig. 2. The biggest discrepancies were in the eutrophic lakes (Sie-a, Ena-a, Loh1-a).

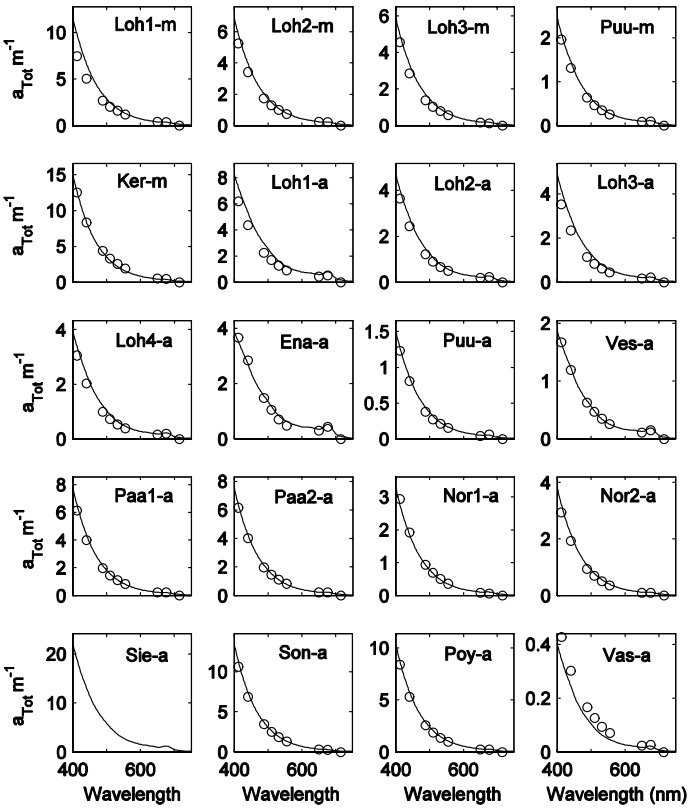

Fig. 1. Simulated (—) and measured (o, with ac-9) total absorption coefficients (a_{tot}) without the contribution of pure water. The measured a_{tot} of Sie-a station were not included due to the non-linearity of the ac-9 measurements. The scale of the x-axis varies by station.

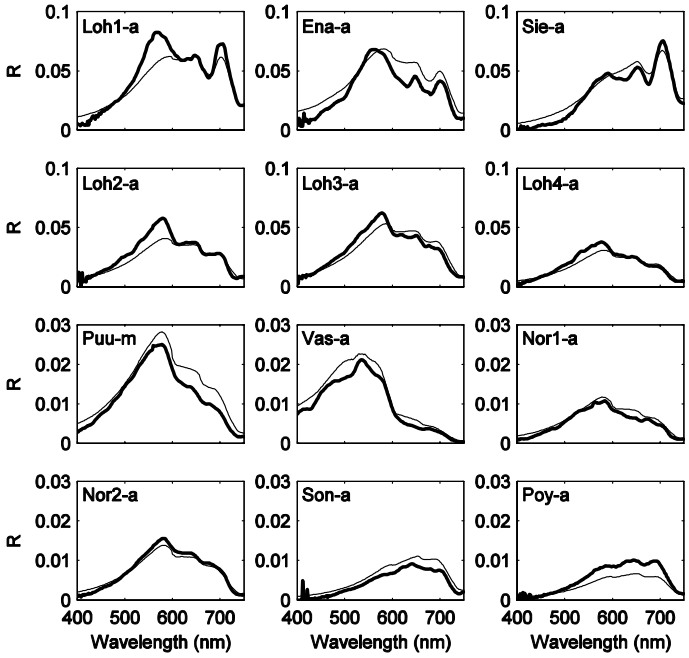

Fig. 2. Measured (▬) and simulated (—) R(λ) of 12 stations. $R^2 = 0.921$, rmse = 24.8%.

Table 4. The coefficients of the reflectance model.

Coefficient	Symbol	Value	Source
Absorption coefficient of pure water	$a_w(\lambda)$	see the reference	*Buiteveld* (1994)
Specific absorption of phytoplankton	$a^*_{ph}(\lambda)$	see the reference	*Ylöstalo et al.* (2005)
Slope factor of CDOM absorption	S_{CDOM}	0.0150 nm^{-1}	18 stations of this study
Specific absorption of bleached TSS at 400 nm	$a^*_{TSS}(400)$	0.13 l $m^{-1}mg^{-1}$	*Ylöstalo et al.* (2005)
Slope factor of tripton absorption	S_{tri}	0.012 nm^{-1}	*Ylöstalo et al.* (2005)
Specific scattering of TSS at 555 nm	$b^*_{TSS}(555)$	0.811 l $m^{-1}mg^{-1}$	13 stations of this study
Scattering exponent of TSS	n_b	0.705	14 stations of this study
Scattering coefficient of pure water	$b_w(\lambda)$	see the reference	*Buiteveld* (1994)
Backscattering probability of pure water	bp_w	0.5	*Sathyendranath et al.* 1989
Backscattering probability of TSS	bp_{TSS}	0.0131	12 stations of this study

3.2 Estimation of water quality

The weight term $(1/2\sigma_i^2)$ in the constrained minimization problem of the inversion method (Eq. 14) was obtained by calculating the rmse(λ) between the measured and simulated R(λ) (Fig. 3). The rmse was highest at 560, 630 and 700 nm, mainly due to the discrepancies in the measured and simulated R in the mesotrophic and eutrophic stations.

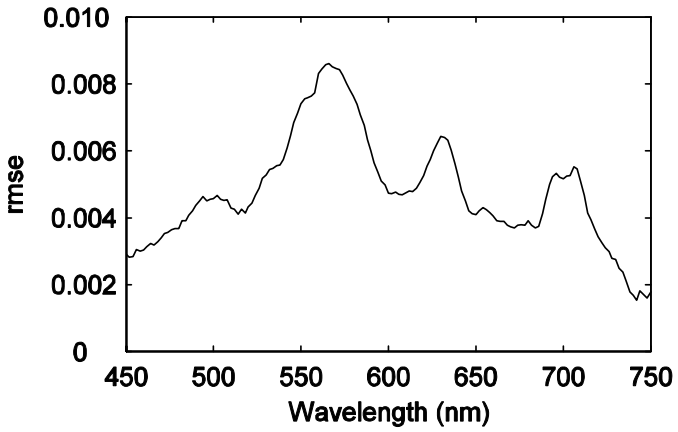

Fig. 3. rmse between the measured and simulated R(λ).

The statistical accuracy characteristics of the inversion based water quality estimates are presented in Table 5. The results were examined mainly by using the rmse, which in our dataset was more sensitive to the accuracy differences than R^2. The results from the MERIS and MODIS inversions were very similar (Fig. 4). In the case of C_{TSS} and $a_{cdom}(400)$ the rmse was slightly lower for MERIS than for MODIS. Both MERIS and MODIS inversions overestimated the highest $a_{cdom}(400)$ (Sie-a). In case of $C_{Chl\text{-}a}$ the high concentrations were estimated accurately, but at the low concentrations the correlation was low. The estimation accuracies with the MERIS and MODIS inversions

were almost as good as in the inversion that used the whole reflectance spectrum with a 2 nm step (Fig. 5). The three highest values of C_{TSS} and $C_{Chl\text{-}a}$ were clearly underestimated in the ETM+ based inversion (Fig. 4), but C_{TSS} below 10 mg l^{-1} were in general estimated accurately. The best overall results with ETM+ inversion were obtained for $a_{cdom}(400)$ that yielded a rmse only slightly lower than in case of MERIS and MODIS.

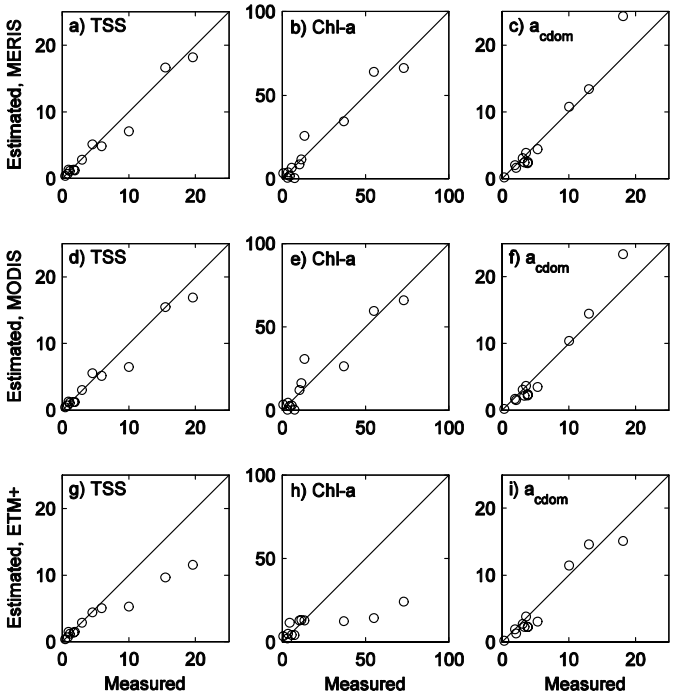

Fig. 4. Measured and estimated OAS with the inversion method using MERIS channels 2-10 (a-c), MODIS channels 2-8 (d-f) and ETM+ channels 1-3 (g-i).

In the empirical algorithm study, the correlation between C_{TSS} and $R(\lambda)$ increased with longer wavelengths (until the 700–730 nm region). The best correlation was obtained with MERIS channel 700-710 nm (rmse=18.1%, R^2=0.978, Fig. 6, Table 6). In case of MODIS, the channel at 747 nm yielded the highest correlation with C_{TSS} (rmse=22%, R^2=0.968) The correlation of the ETM+ channel 630-690 nm with C_{TSS} was lower than in case of the mentioned MERIS and MODIS channels. The best correlation of $C_{Chl\text{-}a}$ was obtained with the MERIS channel ratio R_{705}/R_{665} (rmse=27%, R^2=0.958). The MODIS channel ratio R_{747}/R_{667} yielded clearly lower correlations (rmse=41%, R^2=0.904). In case of ETM+, $C_{Chl\text{-}a}$ could be approximately estimated with the same empirical algorithm as C_{TSS} (based on the 630-690 nm channel, Fig. 6(h)), which can be explained by the strong correlation (R^2 = 0.98, n=12) between $C_{Chl\text{-}a}$ and C_{TSS}. Several channel ratios between reflectance in the 620-730 nm range and R in the 445-600 nm range yielded high correlations with $a_{cdom}(400)$. The ratio between R centered in the 660–667 nm and R centered in the 485–490 nm resulted in the lowest rmse (13–16%, Fig. 6, Table 6) for all three channel configurations.

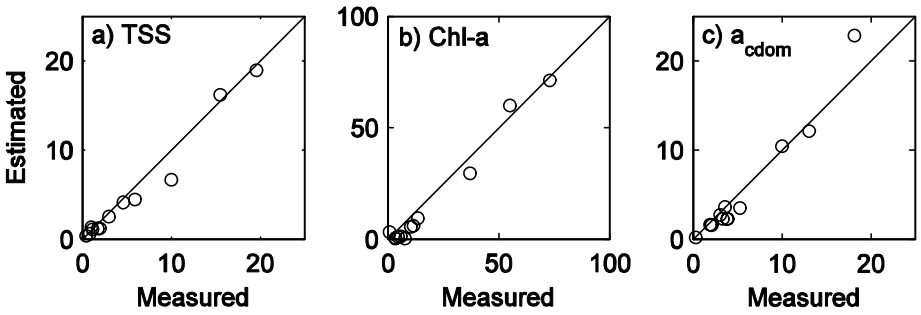

Fig. 5. Measured and estimated OAS with the inversion method using the whole spectrum (450-750 nm).

Table 5. Statistical accuracy characteristics of the inversion based estimates. The correlations are shown in Figs. 4 and 5.

Variable	Channel configuration	R^2	rmse %
C_{TSS}	Full spectrum	0.974	20.7
	MERIS	0.973	19.8
	MODIS	0.966	25.0
	ETM+	0.967	58.8
$C_{Chl\text{-}a}$	Full spectrum	0.980	25.0
	MERIS	0.943	29.1
	MODIS	0.903	37.3
	ETM+	0.659	105.6
$a_{cdom}(400)$	Full spectrum	0.964	28.8
	MERIS	0.968	34.0
	MODIS	0.975	31.6
	ETM+	0.933	25.9

Table 6. Empirical algorithms with statistical accuracy characteristics. The correlations are shown in Fig. 6.

Variable	Channel configuration	Algorithm	R^2	rmse %
C_{TSS}	MERIS	$C_{TSS} = 247\ R_{700\text{-}710} - 0.506$	0.978	18.1
	MODIS	$C_{TSS} = 811\ R_{743\text{-}750} - 0.116$	0.968	21.8
	ETM+	$C_{TSS} = 324\ R_{630\text{-}690} - 2.08$	0.820	51.9
$C_{Chl\text{-}a}$	MERIS	$C_{Chl\text{-}a} = 76.7\ R_{700\text{-}710}/R_{660\text{-}670} - 52.7$	0.958	26.7
	MODIS	$C_{Chl\text{-}a} = 186\ R_{743\text{-}750}/R_{662\text{-}672} - 27.6$	0.904	41.3
	ETM+	$C_{Chl\text{-}a} = 1120\ R_{630\text{-}690} - 7.30$	0.720	69.1
$a_{cdom}(400)$	MERIS	$a_{cdom}(400) = 2.96\ R_{660\text{-}670}/R_{485\text{-}495} - 0.588$	0.979	14.2
	MODIS	$a_{cdom}(400) = 2.94\ R_{662\text{-}672}/R_{483\text{-}493} - 0.659$	0.980	13.6
	ETM+	$a_{cdom}(400) = 3.03\ R_{630\text{-}690}/R_{450\text{-}520} - 1.19$	0.974	15.9

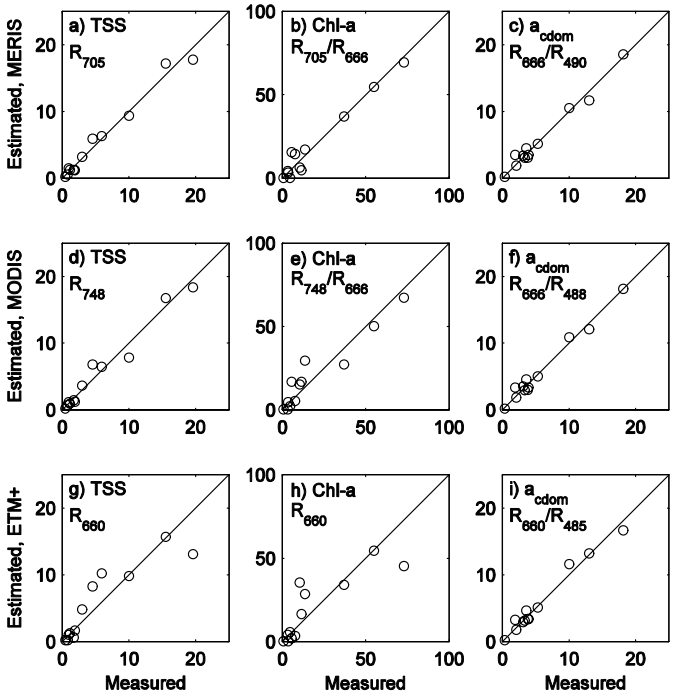

Fig. 6. Measured and estimated OAS by empirical algorithms using the channels of MERIS (a-c), MODIS (d-f) and ETM+ (g-i). The channel or channel ratio applied is shown in each subfigure.

The analyses of all possible two channel ratios and single channels of the full reflectance spectrum (450–750 nm with a step of 2 nm) did not reveal any new C_{TSS} and C_{CDOM} algorithms that would have been more accurate than the best algorithms using the satellite instrument channels. With regard to $C_{Chl\text{-}a}$, the introduction of the 665–675 nm channel ($C_{Chl\text{-}a} = 65.3\ R_{700\text{-}710}/R_{665\text{-}675} - 43.8$) resulted in slightly lower rmse (21.7%) than the use of MERIS channel ratio($R_{700\text{-}710}/R_{660\text{-}670}$) (rmse=26.7%, Table 6).

4. Discussion

4.1 Reflectance model

This study provided extensive data for testing the bio-optical reflectance model, because of large differences in water quality between the lakes. Our objective was to construct a model that could be used as an interpretation tool in applying remote sensing techniques to Finnish lakes in the period July–August. The reflectances were calculated using the concentrations of OAS (C_{TSS}, $C_{Chl\text{-}a}$ and $a_{cdom}(400)$) at each station, while the SIOPs were assumed to be the same in all lakes (with the exception of $C_{Chl\text{-}a}$ dependent a^*_{ph}).

The ability of the bio-optical reflectance model to simulate the measured reflectance mainly depends on how well the SIOPs are known. The backscattering probability of TSS (bp_{TSS}=0.0131) was estimated here by calibrating the model against

measured reflectances. This value is close to the value reported for Dutch lakes (0.0157, *Dekker* 1993). The resulting $b^*_{b,TSS}$ (555) of 0.0106 l m^{-1} mg^{-1}, calculated from the backscattering probability and the scattering coefficient, is also in agreement with other lake studies. In the Dutch Lake IJsselmeer, for example, the $b^*_{b,TSS}$ (550) was 0.011 l m^{-1} mg^{-1} (*Hoogenboom et al.,* 1998a), and *Heege and Fischer* (2004), assuming wavelength independent backscattering, reported a specific backscattering coefficient of 0.0086 l m^{-1} mg^{-1} for Lake Constance, Germany.

The biggest discrepancies in the reflectance simulations were in the eutrophic lakes, namely Enäjärvi, Sierijärvi and at station Loh1-a of Lake Lohjanjärvi. (Fig. 2). This may be due to the fact that in eutrophic lakes the absorption and backscattering properties of phytoplankton have a strong impact on the reflectance. These properties can differ considerably depending on the dominating phytoplankton species, but they could not be taken into account in the model because the lake specific SIOPs of phytoplankton were not available. Here we used the average, $C_{Chl\text{-}a}$ dependent $a^*_{ph}(\lambda)$ (Eq. 12) of Finnish lakes in August conditions, although $a^*_{ph}(\lambda)$ can vary according to the species composition, the physiological state of phytoplankton and the prevailing light conditions. In the eutrophic lakes of this study the phytoplankton species composition was diverse. For example, in Lake Lohjanjärvi (Loh1-a) and in Lake Sierijärvi (Sie-a) the phytoplankton biomass was dominated by two cyanobacteria: *Nostocales* (83% of the biomass) and *Chroococcales* (72%), respectively. By contrast, in Lake Enäjärvi photoplankton was more heterogeneous: *Dinophyta* (28%), *Chroococcales* (24%), *Nostocales* (19%), and *Chlorophyceae* (19%).

Backscattering was here calculated without the separation of total particles into tripton and phytoplankton. The specific backscattering coefficient of phytoplankton can vary between phytoplankton species due to the variations in shape and in refractive index of phytoplankton cells. For example, cyanobacteria with gas-vacuoles have high scattering coefficients (*Ganf et al.,* 1989). Unfortunately, however, direct measurements of scattering properties of phytoplankton are few. As a consequence, the estimation of backscattering properties of phytoplankton in bio-optical modeling of lakes (*Dekker,* 1993; *Kutser,* 1997; *Strömbeck,* 2001) has mainly been based on the research results of the ocean phytoplankton (e.g. *Morel,* 1980; *Sathyendranath et al.,* 1989; *Ahn et al.,* 1992).

The model seems to overestimate reflectance in the short wavelength region (400–450 nm). The measured reflectances in this region were not reliable in the lakes with high $a_{cdom}(400)$, because in the short wavelengths the upwelling and downwelling irradiances (due to strong absorption by CDOM) were low and their measurement accuracy was poor. In addition, the upwelling irradiance measurements were not corrected for the instrument self-shading. Self-shading leads to underestimation of the measured reflectance and it depends on the radius of the instrument, absorption coefficient, solar altitude, and on the ratio between diffuse and direct solar irradiance (*Gordon and Ding* 1992). The correction methods (*Gordon and Ding,* 1992; *Zibordi and Ferrari,* 1995) for instrument self-shading have been mainly developed for the ocean waters and they have not been tested in waters with high CDOM levels. The correction methods also

require knowledge on the ratio between diffuse and direct solar irradiance, which was not available for our field measurements. The error due to self-shading increases with increased absorption. Most of our study lakes have high CDOM concentrations and the biggest error is therefore expected in the blue region of the spectrum. This region (400–448 nm) was not included in the determination of bp_{TSS} and in the inversion calculations.

The slope factor of CDOM absorption used here (0.0150 m^{-1}) lies within the range that has been reported for lakes in Estonia and Finland (mean value 0.016-0.017, *Sipelgas et al.,* 2003) and Sweden (mean value 0.015, *Pierson and Strömbeck,* 2001). The comparison of published S_{CDOM} are, however, difficult because of differences in the wavelength range used in the estimation of S_{CDOM}, in the filter type (pore size) and in the method to correct spectrophotometric measurements for the residual scattering.

4.2 Inversion

In the inversion of full reflectance spectrum, $a_{cdom}(400)$ was overestimated at the most eutrophic station Sie-a (Fig. 5(c), measured $a_{cdom}(400) = 18.2\ m^{-1}$). One explanation for this may be the exceptional $b^*_{b,TSS}(555)$ of Sie-a. Another reason could be the underestimation of the measured R at 450–500 nm arising from the low measurement accuracy of low irradiance levels. This was further confirmed by the use of the 500–750 nm region instead of 450–750 nm in the inversion, which decreased the $a_{cdom}(400)$ estimate from 22.8 m^{-1} to 19.1 m^{-1}. In a study of error propagation on inversion of irradiance reflectance in Lake Constance, *Gege* (2002) concluded that the two most important sources of error in the estimation of $a_{cdom}(400)$ were S_{CDOM} and C_{TSS} . The estimation C_{TSS} was not critically effected by errors of other OAS, but was sensitive to the specific backscattering coefficient.

$C_{Chl\text{-}a}$ was estimated with a lower accuracy than C_{TSS}, and $a_{cdom}(400)$, particularly at low $C_{Chl\text{-}a}$ concentrations. This could be due to the fact that absorption by CDOM shadows the first absorption maximum (at 440 nm) of Chl-a and that the second absorption maximum (at 675 nm) is quite narrow. Also noise in the measured reflectance together with variation in the specific absorption and backscattering properties of phytoplankton can reduce the estimation accuracy of $C_{Chl\text{-}a}$. The low estimation accuracy of $C_{Chl\text{-}a}$ by inversion in 'case-2' waters has also been reported by *Lahet et al.* (2000) and *Gege* (2002). According to *Gege* (2002) $C_{Chl\text{-}a}$ estimation by inversion in Lake Constance was very sensitive to errors in $a_{cdom}(400)$ and S_{cdom} and they must be known with an accuracy of a few percent if a $C_{Chl\text{-}a}$ error of 25% is required.

In our study the estimation accuracy of OAS by inversion is somewhat better than those obtained in similar lake studies with large variations in water quality (*Kutser et al.,* 2001; *Pierson and Strömbeck,* 2001). However, the comparison to those two earlier studies is difficult, because the applied optimisation method and the possible weighting factors for different wavelengths were not described in detail.

4.3 Empirical algorithms

The best empirical C_{TSS} and $C_{Chl\text{-}a}$ algorithms of our study are the same as those found in shipborne and airborne reflectance or radiance measurements in several lake regions (e.g. *Millie et al.,* 1992; *Dekker,* 1993; *Gitelson et al.,* 1993; *Schalles et al.,* 1998; *Kallio et al.,* 2001; *Pierson and Strömbeck,* 2001; *Kallio et al.,* 2003). The widely used NIR/red- ratio (ratio of two channels at about 705 and 670 nm) in the $C_{Chl\text{-}a}$ algorithm is based on the Chl-a related absorption maximum at about 675 nm. The 705 nm wavelength region is a good normalizing channel because absorption by other OAS is low and reflectance is mostly influenced by backscattering. For the same reason the reflectance in the 700-730 nm region is optimal for estimating the C_{TSS}.

The best empirical $a_{cdom}(400)$ algorithm (based on $R_{662\text{-}672}/R_{483\text{-}493}$) confirms the findings of *Pierson and Strömbeck* (2000). Based on the simulated water leaving radiance reflectances of three largest lakes in Sweden, *Pierson and Strömbeck* (2000) concluded that $a_{cdom}(412)$ was best predicted by linear regression against a channel ratio of wavelength > 600 nm to a wavelength in the 400-580 nm range. In one of the lakes studied by *Pierson and Strömbeck* (2000), the use of the Chl-a absorption channel (660-680 nm) yielded higher correlations than the remaining wavelengths at >600 nm. In this algorithm reflection changes due CDOM absorption in the short wavelength region are normalized by changes in reflection not related to CDOM in the longer wavelengths. The 660-680 nm is the best region for normalization, and is probably due to the small variation in reflectance. The increase in reflectance due to increased backscattering by phytoplankton in this region is balanced by the decrease in reflectance due to phytoplankton absorption. Our study shows that even the wide channels of ETM+ (ratio $R_{630\text{-}690}/R_{450\text{-}520}$) yielded almost as low rmse as the narrow channels of MERIS and MODIS in the estimation of $a_{cdom}(400)$. *Kutser et al.* (2004) used a ratio based on the channels 530–610 and 630–690 nm of satellite data (EO-1 ALI) in the regional estimation of CDOM in lakes. They did not use channel 1 (450–520 nm) in the algorithm, because of uncertainties in the atmospheric correction in the blue region of the spectrum. In our experiment the ratio $R_{630\text{-}690}/R_{530\text{-}610}$ yielded a rmse of 44% (R^2=0.80), but without the most eutrophic Lake Sierijärvi the rmse was as low as 14.4% (R^2=0.98).

The strong correlation between OAS can lead to purely empirical algorithms that are not based on the optical properties of the OAS in question and therefore they may not be generally valid. Our dataset was characterized by a strong positive correlation between $C_{Chl\text{-}a}$ and C_{TSS}. Because of this correlation $C_{Chl\text{-}a}$ could be approximately estimated with the same algorithm as C_{TSS} in case of the ETM+ channels. The rest of the best empirical algorithms of this study can be considered as semi-empirical, because they can be explained by the optical properties of OAS.

4.4 Comparison of the channel configurations

MERIS has the best channel configuration of the three tested satellite instruments for the estimation of OAS by the inversion and empirical algorithms in the studied

lakes. In the case of C_{TSS} and $C_{Chl\text{-}a}$ the accuracy of MODIS was close to that of MERIS. The essential difference between MERIS and MODIS is that MERIS has the 705 nm channel, which improves the accuracy of the estimation of C_{TSS} and $C_{Chl\text{-}a}$, particularly when using the empirical algorithms. The channel configuration of MERIS has one additional advantage as compared to MODIS. The 620 nm channel can namely be utilized in the estimation of the cyanobacteria pigment phycocyanin (*Dekker,* 1993; *Simis et al.,* 2005).

The wide channels of ETM+ were less suitable for the estimation of C_{TSS} and $C_{Chl\text{-}a}$ than the narrow channels of MODIS and MERIS. However, the low concentrations of C_{TSS} (< 7 mg l^{-1}) were estimated accurately using the ETM+ inversion. At some stations even the high C_{TSS} were estimated accurately with the empirical ETM+ algorithm based on the ETM+ channel 3 (630–690 nm). Reflectance in this wavelength region is influenced, for example, by the phytoplankton absorption, which probably causes large variation in the accuracy of the estimation of C_{TSS} in meso-eutrophic lakes. The exception in the channel configuration comparison was $a_{cdom}(400)$, which was estimated by the empirical methods and inversion with about the same accuracy for all three instruments. Although the ETM+ channel configuration is designed for land applications, it seems to be suitable for the estimation of $a_{cdom}(400)$ in the boreal lakes.

According to the results MERIS has optimum channels (490, 665 and 705 nm) for the OAS estimation by empirical methods, since the best algorithms using the full spectrum were in practice the same as in case of MERIS. In the inversion the use of the whole spectrum (450-750 nm, 151 channels) instead of the MERIS channels improved only slightly the estimation accuracy of OAS. It is obvious that the inversion method could be improved if the lake-specific SIOPs were available. The inversion method is also sensitive to the measurement accuracy of the whole reflectance spectrum; in our CDOM rich lakes the measurement of low reflectance at the blue end of the spectrum is problematic.

Our study shows the potential of different channel configurations for estimating OAS. When applying actual remote sensing data for OAS estimations, the overall results are additionally affected by atmospheric disturbance, surface reflectance and instrument characteristics (SNR, radiometric characteristics). The estimation accuracy of the OAS using the actual satellite instrument data, particularly in case of the inversion method, depends additionally on how well these factors can be taken into account when converting the radiance measurements at the instrument level to the subsurface reflectance. The use of the long wavelength channels (e.g. the 747 nm channel of MODIS) for the estimation of C_{TSS} by satellite remote sensing may be difficult, because of the low radiance levels. Short wavelengths (400–450 nm) were not included in our analyses. When working with actual remote sensing data this region can also be problematic due to low radiance of the CDOM-rich lakes and strong disturbance by the atmosphere. Unlike MERIS and MODIS, LANDSAT ETM+ was not designed for water applications. Because of this (e.g. low SNR, 8-bit data) the accuracy decrease can be expected to be higher than in the case of MERIS and MODIS, if actual satellite instrument data is used.

5. Conclusions

In the development of the remote sensing algorithms for water quality estimations in a specific region, there is a need to identify optimum channel configurations and interpretation methods. Such studies should be based on the knowledge of how OAS and their SIOPs influence the reflectance in different parts of spectrum. SIOPs are essential for the inversion method, but they are also important for the development and use of empirical algorithms, for example in selecting the optimum channels and with regard to the limitations of their use in a specific region or season. The lakes in this study represent the boreal region, where CDOM concentrations are typically high, and $C_{Chl\text{-}a}$ and C_{TSS} can vary considerably. The high CDOM levels, for example, mean that CDOM absorption shadow the optical signature of phytoplankton in the blue region of the spectrum rendering the blue/green ratio based $C_{Chl\text{-}a}$ algorithms useless.

Empirical methods usually require *in situ* water sampling in cloudless conditions concurrent with the satellite overpass, but they are simple to apply. Additional advantage of the empirical algorithms is that OAS can be estimated employing just a few channels (e.g. the MERIS channels 490, 665, 705 nm). The applicability of the 705 nm channel, important for $C_{Chl\text{-}a}$ and C_{TSS} estimations, has been proved by airborne remote sensing (e.g. *Dekker,* 1993; *Kallio et al.,* 2001), but the usability of this channel as measured from the space needs to be established. According to our results empirical algorithms were in general more accurate than the inversion method. The difference was most evident in the case of $a_{cdom}(400)$. However, the results obtained here are preliminary, because of the low number of stations and because the same dataset was used in model calibration and in testing the algorithms. Therefore, the algorithms presented here should be further tested with an independent dataset.

The inversion method requires knowledge of the SIOPs, which should be preferably determined for each lake. The inversion also calls for a proper atmospheric correction of the satellite images. Unfortunately, the standard atmospheric corrections of the ocean colour instruments are not directly valid for areas such as the boreal region, where OAS concentrations are often high and atmospheric characteristics differ from those assumed for the standard atmospheric corrections (e.g. *Ruddick et al., 2000*; *Siegel et al.,* 2000). The advantage of the inversion method is, on the other hand, that once the SIOP's (lake specific, seasonal) have been determined the inversion can be applied to satellite data without concurrent reference measurements of the OAS concentrations.

Ocean colour instruments such as MERIS and MODIS provide images on a daily basis, but their spatial resolution is suitable only for large lakes. This presents problems in Finland, where although the total number of lakes is about 56 000, most are small (95% of the lakes have an area < 1 km^2). However, the next generation ETM+ instrument, namely ALI, with its improved radiometric characteristics and a spatial resolution of 30 m, might be suitable for estimating C_{TSS} (although not in eutrophic lakes) and C_{cdom}.

Acknowledgements

We would like to thank Antti Herlevi of the University of Helsinki, Division of Geophysics, for making the Li1800UW and ac-9 measurements. Juhani Henttonen and Jouni Satokangas are acknowledged for their contributions to the the field measurements. We are also grateful to Tiit Kutser, the University of Uppsala, Department of Limnology, who helped us with the first stages of the model development. This study was a part of the Satellite Remote Sensing for Lake Monitoring (SALMON) Project funded by the European Union (ENV4-CT96-0311).

References

Ahn, Y.-H., A. Bricaud and A. Morel, 1992. Light backscattering efficiency and related properties of some phytoplankters, *Deep-Sea Research*, **39**, 1835-1855.

Bricaud, A., A. Morel and L. Prieur, 1981. Absorption by dissolved organic matter of the sea (yellow substance) in the UV and visible domains, *Limnology and Oceanography*, **26**, 43-53.

Bricaud, A., M. Babin, A. Morel and H. Claustre, 1995. Variability in the chlorophyll-specific absorption coefficients of natural phytoplankton: Analysis and parametrization, *Journal of Geophysical Research*, **100 (C7)**, 13321-13332.

Buiteveld, H., J.H.M. Hakvoort and M. Donze, 1994. The optical properties of pure water, *Proceedings of the Ocean Optics XII Conference*, Soc. Photoopt. Inst. Eng., **2258**, 174-183.

Bukata, R.P., J.H. Jerome, J.E. Bruton, S.C. Jain and H.H. Zwick, 1981. Optical water quality model of Lake Ontario 2: Determination of chlorophyll a and suspended mineral concentration of natural waters from submersible and low altitude optical sensors, *Applied Optics*, **20**, 1704-1714.

Dekker, A.G., 1993. *Detection of optical water quality parameters for eutrophic waters by high resolution remote sensing.* PhD Thesis. Vrije Universiteit, Amsterdam, The Netherlands, 240 pp.

Doerffer, R. and J. Fischer, 1993. Concentrations of chlorophyll, suspended matter and gelbstoff in case II waters derived from satellite Coastal Zone Scanner data with inverse modeling, *Journal of Geophysical Research*, **99**, 7457-7466.

EN 872, 1996. Water Analysis – Determination of suspended solids. European Committee for Standardization.

Gallie, E.A., 1994. Optical calibration parameters for water-colour models from Swan lake, Northern Ontario, *Canadian Journal of Remote Sensing*, **20**, 156-161.

Ganf, G.G, R.L. Oliver and A.E. Walsby, 1989. Optical properties of gas-vacuolate cells and colonies of Microcystis in relation to light attenuation in a turbid, stratified reservoir (Mount Bold Reservoir, South Australia), *Australian Journal of Marine and Freshwater Research*, **40**, 595-611.

Garver, S.A. and D. Siegel, 1997. Inherent optical property inversion of ocean color spectra and its biogeochemical interpretation: 1. Time series from the Sargasso Sea, *Journal of Geophysical Research*, **102**, 18607-18625

Gege, G., 1998. Characterization of the phytoplankton in Lake Constance for classification by remote sensing, *Archiv für Hydrobiologie – Advances in Limnology*, **53**, 179-193.

Gege, P., 2002. Error propagation at inversion of irradiance reflectance spectra in Case-2-waters. *Proceedings of the Ocean Optics XVI Conference*, Santa Fe, New Mexico, November 18-22, 2002. 10 p. [CD-ROM].

Gitelson, A., G. Garbuzov, F. Szilagyi, K.-H. Mittenzwey, K. Karnieli and A. Kaiser, 1993. Quantitative remote sensing methods for real-time monitoring of inland waters quality, *International Journal of Remote Sensing*, **14**, 1269-1295.

Gitelson, A.A, Y.Z. Yacobi, J.F. Schalles, D.C. Rundquist, L. Han, R. Stark and Etzion, D., 2000. Remote estimation of phytoplankton density in productive waters, *Archiv für Hydrobiologie – Advances in Limnology, **55**,* 121-136

Gons, H.J., 1999. Optical teledetection of chlorophyll *a* in turbid inland waters, *Environmental Science & Technology, **33**,* 1127-1132.

Gordon, H.R., Brown, O.B. and Jacobs, M.M., 1975. Computed relationships between the inherent and apparent optical properties of a flat, homogenous ocean, *Applied Optics*, **14**, 417-427.

Gordon, H.R. and K. Ding, 1992. Self-shading of in-water optical instruments, *Limnology and Oceanography,* **37***,* 491–500.

Heege, T. and J. Fischer, 2004. Mapping of water constituents in Lake Constance using multispectral airborne scanner data and a physically based processing scheme, *Canadian Journal of Remote Sensing*, **30**, 77-86.

Herlevi, A., 2002. Inherent and apparent optical properties in relation to water quality in Nordic waters. Ph.D. Thesis, University of Helsinki, *Report series in Geophysics*, **45**, 1-57.

Hoge, F.E. and P.E. Lyon, 1996. Satellite retrieval of inherent optical properties by linear matrix inversion of oceanic radiance models: An analysis of model and radiance measurement errors, *Journal of Geophysical Research*, **101**, 16631-16648.

Hoogenboom, H.J., A.G. Dekker, IJ.A. Althuis, 1998a. Simulation of AVIRIS sensitivity for detecting chlorophyll over coastal and inland waters, *Remote Sensing of Environment*, **65**, 333-340.

Hoogenboom, H.J., A.G. Dekker and J.F. De Haan, 1998b. Retrieval of chlorophyll a and suspended matter in inland waters from CASI data by matrix inversion, *Canadian Journal of Remote sensing*, **24**, 144-152.

ISO 10260, 1992. Water quality – Measurement of biochemical parameters – Spectrometric determination of the chlorophyll a concentration. International Organization for Standardization.

Jerlov, N.G., 1976. *Marine optics*. Elsevier, Amsterdam, 231 pp.

Kallio, K., S. Koponen and J. Pulliainen, 2003. Feasibility of airborne imaging spectrometry for lake monitoring - a case study of spatial chlorophyll a distribution in two meso-eutrophic lakes. *International Journal of Remote Sensing*, **24**, 3771-3790.

Kallio, K., T. Kutser, T. Hannonen, S. Koponen, J. Pulliainen, J. Vepsäläinen and T. Pyhälahti, 2001. Retrieval of water quality variables from airborne spectrometry of various lake types in different seasons. *The Science of The Total Environment*, **268**, 59-77.

Kirk, J., 1984. Dependence of relationship between inherent and apparent optical properties of water on solar altitude, *Limnology and Oceanography*, **29**, 350-356.

Kloiber, S.M., P.L. Brezonik, L.G. Olmanson and M.E. Bauer, 2002. A procedure for regional lake water clarity assessment using Landsat multispectral data, *Remote Sensing of Environment*, **82**, 38-47.

Kondratyev, K.Ya, D.V. Pozdnyakov and L.H. Pettersson, 1998. Water quality remote sensing in the visible spectrum, *International Journal of Remote Sensing*, **19**, 957-979.

Kutser, T., 1997. Estimation of water quality in turbid inland and coastal waters by passive optical remote sensing. PhD Thesis, *Dissertationes Geophysicales Universitatis Tartuensis*, **8**, University of Tartu, Estonia, 69 pp.

Kutser, T., A. Herlevi, K. Kallio and H. Arst, 2001. A hyperspectral model for interpretation of passive optical remote sensing data, *The Science of the Total Environment*, **268**, 47-58.

Kutser, T., D.C. Pierson, L. Tranvik, A. Reinart, S. Sobek and K. Kallio, 2004. Estimating the colored dissolved organic matter absorption coefficient in lakes using satellite remote sensing, *Ecosystems* (in print).

Lahet, F., S. Ouillon and P. Forget, 2000. A Three-Component Model of Ocean Color and Its Application in the Ebro River Mouth Area, *Remote Sensing of Environment*, **72**, 181-190.

Lavery, P., C. Pattiaratchi, A. Wyllie and P. Hick, 1993. Water quality monitoring in estuarine waters using the landsat thematic mapper, *Remote Sensing of Environment*, **46**, 268-280.

Lee, Z. and K.L. Carder, 2004. Absorption spectrum of phytoplankton pigments derived from hyperspectral remote-sensing reflectance, *Remote Sensing of Environment*, **89**, 361-368.

Maritorena, S., D.A. Siegel and A.R. Peterson 2000. Optimization of a semianalytical ocean color model for global-scale applications, *Applied Optics*, **41**, 2705-2714.

Millie, D.F., M.C. Baker, C.S. Tucker, B.T. Vinyard and C.P. Dionogi, 1992. High-resolution airborne remote sensing of bloom-forming phytoplankton, *Journal of Phycology*, **28**, 281-290.

Morel, A., 1980. In water and remote measurements of ocean color, *Boundary-Layer Meteorology*, **18**, 177-201.

Nelder, J.A. and R. Mead, 1965. A simplex method for function minimization, *Computer Journal, 7,* 308-313.

OECD, 1982. Eutrophication of water, Monitoring, Assessment and Control. Paris, 150 pp.

O'Reilly, J.E.. S. Maritorena, G. Mitchell, D. Siegel, K. Carder, S. Garver, M. Kahru and C. Mcclain, 1998. Ocean color chlorophyll algorithm for SeaWiFS, *Journal of Geophysical Research*, **103***,* 24937-24953.

Pierson, D.C. and N. Strömbeck, 2000. A modelling approach to evaluate preliminary remote sensing algorithms: Use of water quality data from Swedish Great Lakes, *Geophysica*, **36***,* 177-202.

Pierson, D. and N. Strömbeck, 2001. Estimation of radiance reflectance and the concentrations of optically active substances in Lake Mälaren, Sweden, based on direct and inverse solutions of a simple model, *The Science of the Total Environment*, **268**, 171-188.

Pozdnyakov, D.V., K.Ya. Kondratyev, R.P. Bukata and J.H. Jerome, 1998. Numerical modeling of natural colour: implications for remote sensing and limnological studies, *International Journal of Remote Sensing*, **19***,* 1913-1932.

Roesler, C.S., M.J. Perry and K.L. Carder, 1989. Modeling in situ phytoplankton absorption from total absorption spectra, *Limnology and Oceanography*, **34***,* 1512-1525.

Ruddick, K.G., F. Ovidio and M. Rijkeboer, 2000. Atmospheric correction of SeaWiFS imagery for turbid coastal and inland waters, *Applied Optics*, **39**, 897–912.

Sathyendranath, S., L. Prieur and A. Morel, 1989. A three component model of ocean colour and its application to remote sensing of phytoplankton pigments in coastal waters, *International Journal of Remote Sensing*, **10**, 1373-1394.

Schalles J. F., A.A. Gitelson, Y.Z. Yacobi and A.E. Kroenke, 1998. Estimation of chlorophyll *a* from time series measurements of high spectral resolution reflectance in a eutrophic lake, *Journal of Phycology*, **34**, 383-390.

Schiller, H. and R. Doerffer, 1999. Neural network for emulation of an inverse model operational derivation of Case II water properties from MERIS data, *International Journal of Remote Sensing*, **20**, 1735-1746

Siegel, D.A., Wang, M., Maritorena, S. and Robinson, W., 2000. Atmospheric correction of satellite ocean color imagery: The black pixel assumption, *Applied Optics*, **39***,* 3582-3591.

Simis, S.G.H., S.W.M. Peters and H.J. Gons, 2005. Remote sensing of the cyanobacterial pigment phycocyanin in turbid inland water, *Limnology and Oceanography*, **50**, 237-245.

Sipelgas, L., H. Arst, K. Kallio, A. Erm, P. Oja and T. Soomere, 2003. Optical properties of dissolved organic matter in Finnish and Estonian lakes, *Nordic Hydrology,* **34**, 361-386.

Strömbeck, N., 2001. Water quality and optical properties of Swedish lakes and coastal waters in relation to remote sensing. Ph.D Thesis, Uppsala University, *Comprehensive Summaries of Uppsala dissertations from the faculty of science and technology*, **633**, 1-27

WET Labs, 1995. *ac-9 Users Manual*. Philomath, Oregon, USA.

Vincenta, R.K., X. Qina, R.M.L. McKayb, J. Minerb, K. Czajkowskic, J. Savinod and T. Bridgemand, 2004. Phycocyanin detection from LANDSAT TM data for mapping cyanobacterial blooms in Lake Erie, *Remote Sensing of Environment*, **89**, 381-392.

Ylöstalo, P., K. Kallio and J. Seppälä, 2005. Absorption properties of particles and CDOM in lake waters. (in prep.)

Zibordi, G. and G.M. Ferrari, 1995. Instrument self shading in underwater optical measurements: Experimental data, *Applied Optics*, **34**, 2750-2754.